CLOUD SCENE SIMULATION MODEL (CSSM)

Susan A. Triantafillou

Northeast Consortium for Engineering Education
68 Port Royal Square
Port Royal, VA 22535

August 2000

Scientific Report
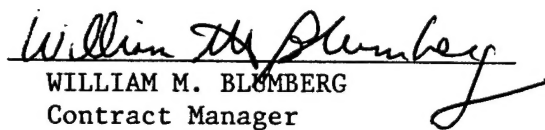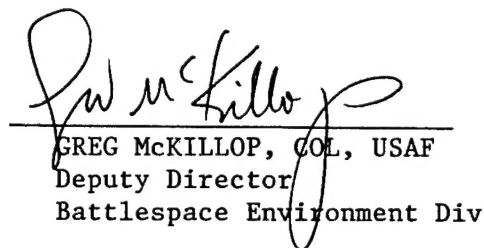
20020619 007

AIR FORCE RESEARCH LABORATORY
Space Vehicles Directorate
29 Randolph Road
AIR FORCE MATERIEL COMMAND
HANSCOM AIR FORCE BASE MA 01731-3010

"This technical report has been reviewed and is approved for publication"

_____
WILLIAM M. BLOMBERG
Contract Manager

_____
GREG McKILLOP, COL, USAF
Deputy Director
Battlespace Environment Div

REPORT DOCUMENTATION PAGE

1. REPORT DATE (DD-MM-YYYY)	2. REPORT TYPE	3. DATES COVERED (From - To)
31 Aug 2000	Interim	

4. TITLE AND SUBTITLE

Cloud Scene Simulation Model (CSSM)

5a. CONTRACT NUMBER
F19628-98-C-0029

5b. GRANT NUMBER

5c. PROGRAM ELEMENT NUMBER
62101F

6. AUTHOR(S)

Susan A. Triantafillou

5d. PROJECT NUMBER
9993

5e. TASK NUMBER
GS

5f. WORK UNIT NUMBER
PE

7. PERFORMING ORGANIZATION NAME(S) AND ADDRESS(ES)

Northeast Consortium for Engineering Education
68 Port Royal Square
Port Royal, VA 22535

8. PERFORMING ORGANIZATION REPORT NUMBER

9. SPONSORING / MONITORING AGENCY NAME(S) AND ADDRESS(ES)

Air Force Research Laboratory/VSB
29 Randolph Rd.
Hanscom AFB MA 01731-3010

10. SPONSOR/MONITOR'S ACRONYM(S)

11. SPONSOR/MONITOR'S REPORT NUMBER(S)
AFRL-VS-TR-2002-1561

12. DISTRIBUTION / AVAILABILITY STATEMENT

Approved for public release: distribution unlimited

13. SUPPLEMENTARY NOTES

14. ABSTRACT

The majority of the effort focussed on fine tuning the Cloud Scene Simulation Model(CSSM). Support was also provided for the National Polar Orbiting Operational Environmental Satellite System (NPOESS) by determining NPOESS Environmental Data Records accuracy requirements.

15. SUBJECT TERMS

Phillips Laboratory Scholar Program, CSSM, real cloud imagery, NPOESS, EDR, accuracy requirements

16. SECURITY CLASSIFICATION OF:			17. LIMITATION OF ABSTRACT	18. NUMBER OF PAGES	19a. NAME OF RESPONSIBLE PERSON
a. REPORT	b. ABSTRACT	c. THIS PAGE			William A.M. Blumberg
Unclassified	Unclassified	Unclassified	Unlimited	25	19b. TELEPHONE NUMBER (include area code) 781-377-3601

CONTENTS

LIST OF FIGURES

LIST OF TABLES

1 SUMMARY OF THE YEAR'S WORK

This report reviews the work done under contract F19628-98-C-0029. Most of my time was spent on a project that focussed on tuning the Cloud Scene Simulation Model (CSSM). This is described briefly below and in greater detail in the next section. Other projects in which I participated involved the National Polar-Orbiting Operational Environmental Satellite System (NPOESS), CSSM Statistics, and satellite cloud support. These are discussed below.

The CSSM tuning project was done in cooperation with Steven M. Ayer, Sara C. Gordon, Joel B. Mozer, and Guy Seeley. The CSSM approximates clouds in terms of appearance and water content. The project aimed to assess the model's clouds in terms of radiometric accuracy. A measurement of radiometric accuracy was established and used for this assessment. Parameter adjustments were made to improve the CSSM's radiometric predictions.

The CSSM tuning project is discussed in Section 2 of this report. A more complete discussion can be found in the project report [1]. I co-authored and edited this report and also wrote a paper on the subject for presentation at the Simulation Interoperability Workshop. The areas of the project to which I made significant contributions are treated in detail in Sections 2.3 − 2.5. My collaborators are primarily responsible for the work described in Sections 2.2.2 − 2.2.4.

The NPOESS project was carried out by David J. Smalley, Joel B. Mozer, and myself. A complete discussion of the project can be found in [6]. NPOESS is targeted to be operational in 2010 and to produce Environmental Data Records (EDRs), which are expected to have military applications. For this study, selected EDRs were used to predict Lock-On-Range (LOR) of an infrared weapon. In question was the accuracy required in the EDRs to obtain a good prediction of LOR.

My contribution was made at the early stages to the plan of study. I proposed viewing the problem in terms of a space spanned by the EDR accuracies. Calculations would be done to find the variation of LOR accuracy in that space. Several ways of stepping through the space and accounting for costs associated with improving an EDR accuracy were offered. An outcome of using this approach would be a path through the EDR accuracy space that could be interpreted as a set of instructions for improving EDR accuracies in order of importance.

As the project progressed in my absence (during my maternity leave), some modifications to the original plan were made in light of the intermediate

results. A conclusion of the study was that the horizontal resolution of the mixing ratio and the water vapor mixing ratio were the two most important values to measure accurately for the purposes of predicting LOR.

There were two additional projects to which I made small contributions. I analyzed data for the CSSM Statistics project. And I ran the Mesoscale Model 5 for several scenarios for a satellite cloud support project.

2   CSSM TUNING

2.1   INTRODUCTION

Current applications of the Cloud Scene Simulation Model (CSSM) fall into two categories. The first is the generation of visually realistic depictions of clouds, that are consistent with a given set of meteorological conditions. Applications in this category include flight simulation, mission planning, virtual training, and situational awareness. The second category of application involves more quantitative representation of clouds where accurate effects of clouds on the radiation field are required. Examples include sensor simulation, target background clutter simulation and infrared scene prediction.

The former category of application generally requires that the clouds generated by the CSSM be qualitatively cloud-like and that the visualization of those clouds be aesthetically consistent with the end-user's conception of real atmospheric clouds. To achieve this goal, the relevant free parameters of the CSSM have been chosen as a function of cloud type to produce the most realistic clouds possible. Absolute accuracy of the magnitude of the cloud liquid water content (CLWC) fields is of secondary importance in such applications.

The second class of application presents a more stringent set of requirements for the data output by the CSSM. Generally, for uses where the CSSM fields form the basis of further calculations and quantitative studies, more rigor must be applied to both the estimation of model parameters, and the post processing of the CLWC fields produced by the CSSM. Accuracy and physical consistency are most important in this type of application.

For the present work, we are concerned only with the latter class of problems and will confine ourselves to cases where the quantitative information required by the user involves the interaction of visible and infrared radiation with the clouds. This is the case, for example for the construction of

a two-dimensional scene that includes clouds for evaluating the response of an infrared missile seeker. In these types of problems, the raw CLWC data must be transformed into optical (or radiometric) properties, which can in turn be used as input to a radiative transfer calculation.

A goal of the current study is to evaluate the radiometric accuracy of CSSM clouds. Once this is established an effort will be made to improve the accuracy by selectively adjusting CSSM parameters. Finally, the applicability of the adjusted CSSM will be assessed for a more general case.

These goals were achieved by coupling the CSSM with radiative transfer models and performing a quantitative comparison between the resulting synthetic images and real-cloud images. Section 2.2 gives the background on the models, the real-cloud imagery, and the quantifying methods used. The CSSM adjustments are discussed in Section partune and the effects of making these adjustments are discussed in Section sensitive. Results and conclusions are given in Section results.

2.2   BACKGROUND

2.2.1   CSSM

The Cloud Scene Simulation Model (CSSM) was developed by TASC of Reading, MA for the Air Force Research Laboratory. It generates high-fidelity, synthetic fields of cloud liquid water content (CLWC) in four dimensions (three spatial dimensions and time). The CSSM supports modeling and simulation activities where such cloud fields are required. The scales addressed by the CSSM cloud fields correspond to characteristic of "out-the-cockpit" scales. Typical domains are $1 - 100$ km with spatial resolutions of $1 - 100$ m and a temporal resolution of $1 - 100$ minutes.

The core algorithms of the CSSM are based on the fractal Rescale and Add (RSA) method [5]. This algorithm relies on a multidimensional lattice of random numbers, which can be produced using a random number seed. From the random number lattice the RSA method generates a multidimensional lattice of values that possesses inherent fractal structure as a function of lattice position. A number of parameters determine the general behavior of the function. These parameters include the lattice resolution, summation limits, lacunarity, and Hurst parameter, which may be assigned different values for different cloud types and different directions. The effects of the parameter values are discussed briefly here and in greater detail in Section 2.3.

3

The RSA algorithm is given in [3] and repeated here for completeness. At position $\mathbf{x} = (x_1, x_2, x_3, x_4)$ in the fractal lattice, the RSA has the value

$$V(\mathbf{x}) = \sum_{k=k_0}^{k_1} \frac{1}{r^{kH}} f(r^k \mathbf{y}(\mathbf{x})), \tag{1}$$

where k_0 and k_1 are summation limits, r is lacunarity, H is Hurst parameter, and $f(r^k \mathbf{y}(\mathbf{x}))$ is a function that depends on the position in the random lattice, $\mathbf{y} = (y_1, y_2, y_3, y_4)$, which depends on $\mathbf{x}$. The positions in the random lattice and the fractal lattice are related by

$$y_i = \frac{x_i}{R_i}, \tag{2}$$

where R_i is the lattice resolution in the ith direction. To evaluate $f(r^k \mathbf{y})$ an integer term and a fractional term are calculated. The integer term is

$$d_i = \lfloor r^k y_i \rfloor \operatorname{modulo}(N_i - 1), \tag{3}$$

where N_i is the number of sites in the random lattice in the ith direction, and $\lfloor a \rfloor$ means the integer portion of a. The fractional term is

$$\eta_i = \Delta y_i^2 (3.0 - 2.0 \Delta y_i), \tag{4}$$

where

$$\Delta y_i = r^k y_i - \lfloor r^k y_i \rfloor. \tag{5}$$

The integer and fractional terms are combined to obtain a position in the continuous extension of the random lattice. This position, $\mathbf{Y}$, generally falls between lattice nodes and has components

$$Y_i = d_i + \eta_i. \tag{6}$$

The value of $f(r^k \mathbf{y})$ is the result of linearly interpolating between the random lattice values assigned to the nodes surrounding the position $\mathbf{Y}$.

The values chosen for the fractal parameters in the CSSM can make a significant difference in the outcome of the fractal algorithm. These parameters interact in complicated ways so that the effects of each value cannot always be simply stated. The developers assigned values to the parameters used in the RSA algorithm based on an understanding of how the algorithm works and on numerical experimentation. Some of the results of these experiments

4

were evaluated using numerical tools (such as autocorrelation function analysis) while other results were assessed by visual inspection. The parameters are discussed briefly here and in more detail in Section 2.3.

The lattice resolution is effectively a scale factor used to locate a position in the random lattice, given a position in the fractal lattice (or physical space). As the lattice resolution is increased, a greater number of steps across the fractal lattice are required to take a step in the random lattice and therefore variations in the outcome occur on a larger scale.

The summation limits k_0 and k_1 provide bounds for the spatial scales that are represented by the algorithm. The smallest value of k corresponds to the largest spatial scale and the largest value of k corresponds to the smallest spatial scale.

The lacunarity parameter appears in two places in each term of the RSA algorithm and has two effects on RSA output. The result of these effects in combination is not apparent from inspection of the algorithm. TASC showed through numerical experimentation that for typical values of H and k the net effect of increasing r is an image with more small-scale structure along edges between light and dark regions.

The Hurst parameter, $0 < H < 1$, appears in the coefficient in (1). Assuming that $r > 1$ and $k > 0$, increasing H decreases the amplitude for the given frequency. The magnitude of this effect depends on the values used for k, r, and H. TASC observed that increasing H resulted in clouds with less small-scale variability.

The parameter values used in the CSSM were chosen by an iterative process. Initially, values were set using observations like the ones described above. Algorithm results were judged on either visual or numerical criteria. Then values were adjusted with with the roles of the different parameters in mind. The evaluation and adjustment steps were repeated until satisfactory results were obtained.

The fractal algorithm is applied in three ways, to obtain the horizontal cloud distribution (and cloud top), the cloud base, and the internal water content. The fractal parameters may have different values for each of these three functions as well as different values for each of three directions. Therefore, a total of 27 parameter values could be adjusted to change the outcome of the fractal algorithm.

The RSA algorithm is coupled with other methods that account for meteorological conditions to produce water content data from the RSA's fractal field. These methods are described in [2]. Twelve distinct cloud types can be

produced with the CSSM. For all cloud types other than cumulus, the average water content at a given height within a cloud is assigned as a function of temperature and percent cloud cover using the Feddes model, presented in [4] and also described in [2]. This average water content is combined with RSA output to simulate water content throughout a cloud with realistic variability. For cumulus clouds the relationship between the RSA and the simulated water content is less direct. The RSA introduces variability into the temperature of a cumulus cloud. This local temperature along with a mixing ratio are used by a parcel method to produce water content information. For all cloud types the input required by the CSSM includes meteorological information, a random number seed, domain size, and grid resolution.

2.2.2 RADIATIVE TRANSFER MODELS

CSSM-generated clouds were evaluated in terms of radiative properties. This was achieved by coupling the CSSM to a radiative transfer model through the use of a postprocessor. This is described briefly here and in greater detail in [1].

The Fastmap postprocessor was applied to two-dimensional CSSM images to convert CLWC data into optical properties. This conversion is based on assumed drop size distributions and look-up tables. The optical properties produced include optical depth, extinction coefficient, and single scatter albedo.

The radiative transfer calculation was performed with the Infrared Target Scene Simulation (IRTSS) developed by the Air Force Research Laboratory Weather Impact Decision Aids program. IRTSS renders a texture image by raytracing three-dimensional CLWC and extinction coefficient fields. These fields are products of the CSSM and Fastmap, respectively. IRTSS was used to generate visible waveband cloud scenes, as viewed from the ground directly below.

2.2.3 REAL-CLOUD DATA

Real-cloud data was collected so that comparisons could be made between real and synthetic clouds. Cloud images were taken with a visible band (700 nm) camera using two different lenses during the period July 1995 – February 1997. This resulted in a set of videos from which 962 images were selected automatically by taking every tenth frame. These images were cropped to

obtain 256 × 256 pixel images. An additional set of 96 video images was selected by a meteorologist so that the different cloud types were represented by equal numbers of images.

Real-cloud images were also provided by a field experiment conducted at Hanscom Air Force Base in April – May 1998. For each scene recorded for this field experiment, multiple images were generated to capture different wave bands. For the current study, 146 images from the 684 – 700 nm wave band image collection were selected. Since these images were rectangular and had less than 256 pixels across one direction, 128 × 128 pixel squares were extracted from each of the 146 images.

Meteorological data was collected to correspond to each image. Further details on real-cloud data are in [1]

2.2.4 QUANTIFYING IMAGES

A large number of image-based calculation methods was considered in identifying metrics that could capture the radiometric properties of cloud images. A goal was to be able to characterize an image using a small set of values. Thus a process was needed to select a small set of metrics from many candidates. The assumption was made that metrics that were best at distinguishing between cloud types were the best metrics for capturing the radiometric properties of cloud images.

A two-step process was used to identify the best three-metric combination from a list of 84 candidate metrics. For both of these steps metrics were applied to images of real clouds of various (known) types. A multiple discriminant analysis (MDA) was applied to test the capabilities of the metrics to classify the images. All 84 metrics were considered for the first step of the process, which identified the 17 most promising metrics. This reduced list of metrics served as the input for the second step of the process in which all possible three-metric combinations were studied. The combination that identified the cloud types with the smallest error was taken to be the best three-metric combination for measuring radiometric values.

The metric selection process was applied with the two sets of real-cloud imagery discussed in Section 2.2.3. This led to three different three-metric combinations, one for each individual image set and one for both image sets together.

The image sets and the associated three-metric combinations are summarized in Table 1. Note the last entry in the table refers to a set of 1204

7

No. of images	Source	Three-Metric Combination
962	Video	Low freq. FFT, E5L5, sang
146	Field experiment	Low freq. FFT, Medium freq. FFT, sang
1204	All	Low freq. FFT, Medium freq. FFT, sang

Table 1: Three-metric combinations selected for different sets of images

images which includes the 962 automatically selected video images, the 146 field experiment images, and the the 96 meteorologist-selected video images. The "Low freq. FFT" and the "Medium freq. FFT" are metrics based on coefficients from a fast Fourier transform. They are computed by combining selected coefficients from the low or medium frequency terms, as indicated by the metric name. The E5L5 metric is the result of convolving an image with a kernel designed to detect edges and the levels of intensity in the image. The sang metric is a sum of angles detected in an image through the use of a pair of convolution masks that detect edges in orthogonal directions.

2.3 PARAMETER VALUES AND RADIOMETRIC ACCURACY

New values for fractal parameters were considered for the purposes of tuning the CSSM to produce more radiometrically accurate clouds. The CSSM developers made observations of the effects of the various fractal parameters on the output of the CSSM [3]. While these observations were of value, the goals of the current investigation required further study and experimentation with parameter values to understand their effects on the selected metrics and therefore the radiometric properties of the synthetic clouds generated.

2.3.1 PREDICTED EFFECTS OF ADJUSTING PARAMETERS

Taking a closer look at the RSA algorithm presented in Section 2.2.1 can lead to some insights as to the effects of the different parameters.

The summation limits control the values taken by the summation index k, which appears in two places in the RSA calculation. In one place, the quantity r^k, where r is lacunarity, is used as a factor in evaluating a location in the random lattice. Assuming $r > 1$, larger values of k correspond to
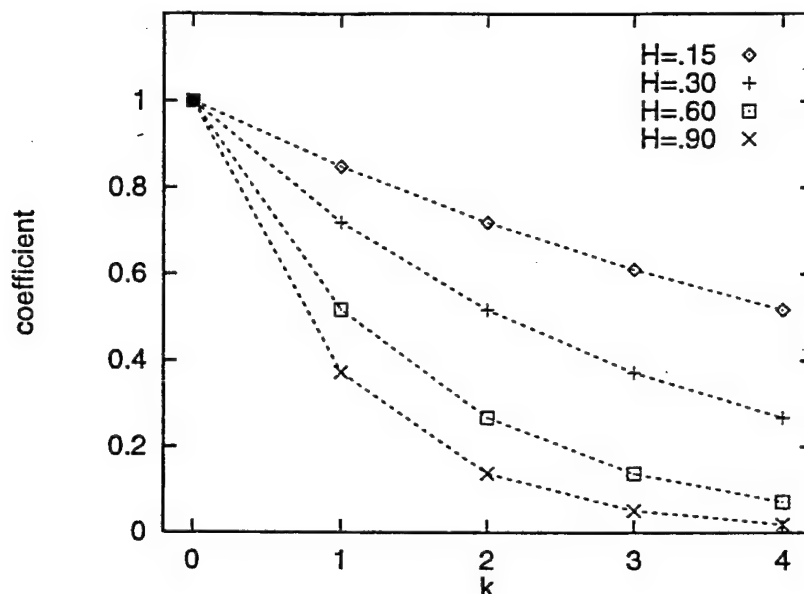
8

Figure 1: The coefficient $\frac{1}{r^{kH}}$ for various values of k and H

higher frequency variation with position. Therefore, larger values of k produce the smaller-scale contributions. The index k is also used to calculate the coefficient of each term in the summation. The coefficient is r^{-kH}, so larger values of k mean smaller coefficients (again assuming $r > 1$). The combined effect of increasing k is that it adds smaller-scale features which are contributed with decreasing magnitude.

Changes in the Hurst parameter, H, produce changes in the coefficient, r^{-kH}. Note that $k = 0$ is the lowest frequency used here and the $k = 0$ coefficient is unaffected by changes in H. For all other frequencies ($k > 0$) the coefficient decreases as H increases. Thus, increasing H causes the lowest frequency term to play a more dominant role. This accounts for the loss of small-scale structure with increasing H observed by the CSSM developers. Other effects of changing H cannot be identified by inspection of the coefficient. These effects are illustrated in Figure 1 which shows coefficients for a range of values of H and typical values of k. The steepness of the segments indicates how quickly the coefficient decreases as k is increased and thus shows the relative importance of subsequent frequencies.

The lacunarity r appears in the RSA in two places. An increase in r
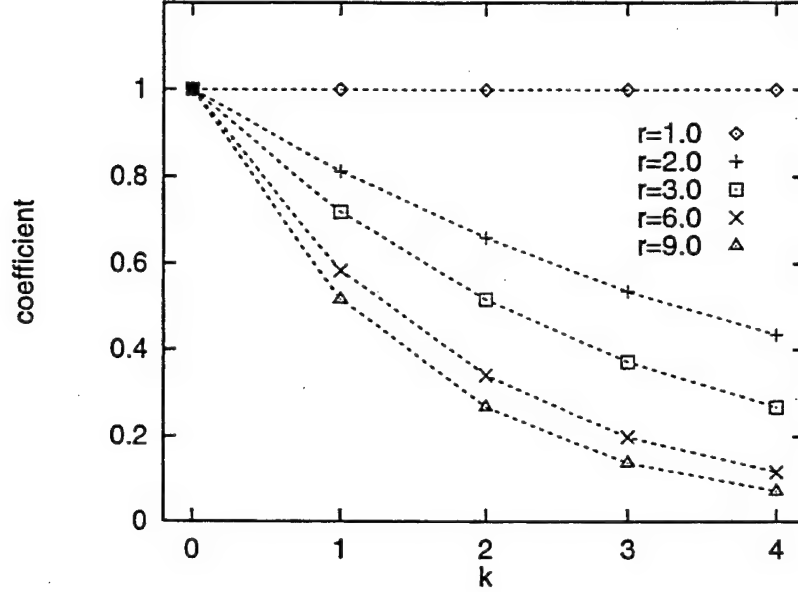
9

Figure 2: The coefficient $\frac{1}{r^{kH}}$ for various values of k and r

produces a decrease in the coefficient, r^{-kH}. As with the Hurst parameter, no generalization can be made as to whether this effect is more or less pronounced as k changes, except for the case where $k = 0$. As r is increased the lowest frequency term (associated with $k = 0$) becomes increasingly more important relative to all other terms. Examples of coefficients are shown in Figure 2 for various values of r and k. In its second role, an increase in r increases the factor that relates the random lattice to the fractal lattice. This has the effect of equating a smaller number of steps across a synthetic cloud with a given number of steps in the random lattice. Another way of looking at this is that it increases all frequencies, except the $k = 0$ frequency. As observed by TASC this leads to more small-scale detail with increasing r. Due to the effect of r on the coefficient noted above, this increased quantity of small-scale detail is of decreasing importance relative to the largest-scale features. The degree to which this occurs can be seen in Figure 2.

Changes in the lattice resolution affect the scaling factor that converts positions from the real lattice into the fractal lattice, as discussed in Section 2.2. Increasing lattice resolution causes variations in the synthetic cloud to occur on a larger scale. This effect is more pronounced for the high-frequency terms

10

in the RSA.

2.3.2 EXPERIMENTING WITH PARAMETER VALUES

As stated in Section 2.2.1, a total of 27 fractal parameter values contribute to the behavior of the fractal lattice produced. To avoid experimenting with such a large number of parameters the different directions were handled by making experimental changes to all directions simultaneously by a single factor. This choice was made under the assumption that the proportions (set by TASC) between the parameters for different directions would be appropriate for adjusted parameter values as well. This left a total of nine candidate parameters for each cloud type that could be adjusted independently.

TASC reported that adjustment of two "key" parameters, the Hurst parameter and the lattice resolution, could be used to "control the character of the resulting cloud field" [2]. Therefore, these parameters were under primary consideration for the current study. The effect of the lacunarity was also explored.

Since radiometric values are closely linked to water content, the RSA functions that most affect water content were of special interest. Cumulus CSSM clouds rely on the RSA algorithm for only two computations, the horizontal cloud distribution (and cloud top) and the cloud base. These results then serve as input into a parcel method calculation which produces the internal water content. Of the two RSA applications, the horizontal parameter values were expected to have more influence on the water content results. Preliminary experiments showed that variation in the horizontal Hurst parameter does not result in a significant change in the radiometric properties of a CSSM cumulus cloud. This may be due to the remote connection between the RSA algorithm and the internal water content in a synthetic cumulus cloud. In order to eliminate this concern, the CSSM clouds generated for the remainder of the study were of stratocumulus type. This choice also had the benefit of speeding up the CSSM computations since the parcel method computations required for cumulus clouds are relatively slow. These were compared to real cumulus clouds.

The fractal parameters expected to have a significant influence on the radiometric properties of CSSM stratocumulus clouds included the parameters used for the internal water content application. Therefore, the internal water content parameters were varied for the current study. The internal water content computation relies on the horizontal cloud distribution, which

Parameter	Values
Internal Hurst parameter	(0.15, 0.15, 0.15), **(0.3, 0.3, 0.3)**, (0.6, 0.6, 0.6), (0.75, 0.75, 0.75), (0.9, 0.9, 0.9)
Internal lattice resolution	(0.3, 0.3, 0.3), (0.6, 0.6, 0.6), **(1.0, 1.0, 1.0)**, (3.0, 3.0, 3.0), (9.0, 9.0, 9.0)
Internal lacunarity	(1.0, 1.0, 1.0), (2.0, 2.0, 2.0), **(3.0, 3.0, 3.0)**, (6.0, 6.0, 6.0), (9.0, 9.0, 9.0)
Horizontal Hurst parameter	(0.15, 0.15, 0.15), **(0.3, 0.3, 0.3)**, (0.6, 0.6, 0 .6), (0.75, 0.75, 0.75), (0.9, 0.9, 0.9)
Horizontal lattice resolution	(2., 2., .333), (4.0, 4.0, 0.666), **(6.0, 6.0 , 1.0)**, (9.0, 9.0, 1.5), (12.0, 12.0, 2.0)
Horizontal lacunarity	(1.0, 1.0, 1.0), (2.0, 2.0, 2.0), **(3.0, 3.0, 3.0)**, (6.0, 6.0 , 6.0), (9.0, 9.0, 9.0)

Table 2: Experimental stratocumulus parameter values. Values are listed for the two horizontal directions and the vertical direction with the original set of values shown in bold.

is based on another RSA application. The parameters associated with this application were also varied.

Wide ranges of values were chosen for experiments with each parameter. This choice was made in order to get some experience with the sensitivity of radiometric values to parameter values. Specific values are shown in Table 2. The values shown in bold are the original parameter values.

Note that while a lacunarity value of 1.0 is used for purposes of this sensitivity study, it is not a sensible choice for other CSSM applications. This is because in the fractal algorithm the lacunarity, r, and the frequency, k, always appear together in the quantity r^k. In order to have distinct frequencies for the different values of k, the quantity r^k must vary with k and thus r must be different than 1.0.

2.4 OBSERVED SENSITIVITY TO PARAMETER CHANGES

By varying one fractal parameter at a time, the sensitivities of the radiometric properties of synthetic clouds to the different parameters could be observed. To assess sensitivity, an error was defined to measure discrepancies between the metric values of real and synthetic clouds. The errors associated with different fractal parameters could then be compared so that error-reducing parameter values could be identified. The results showed that changes in some fractal parameters have a significant effect on the metrics, while others do not.

The metrics used were selected as described in Section 2.2.4 using cumulus real-cloud images. Once selected, the best three-metric combination was used to measure both the real-cloud and synthetic-cloud images. For each metric i, a mean μ_i and standard deviation σ_i among the real clouds was found and used to establish a linear scaling for that metric. The scaling was applied to the synthetic-cloud results producing a measure of error for a particular metric and synthetic cloud. For example, scaling the metric s_i for a given synthetic cloud results in the error

$$e_i = \frac{s_i - \mu_i}{\sigma_i}. \tag{7}$$

The overall error for a synthetic cloud was defined as the L_2 norm[1] of the errors due to the three metrics. The standard deviation in the synthetic-cloud errors was considered when comparing error values.

The synthetic clouds were high resolution stratocumulus (512×512 pixels) images created by coupling CSSM and IRTSS as described in Section 2.2.2. The real clouds were those discussed in Section 2.2.3 and the applicable metrics were given in Section 2.2.4. For each set of real cumulus clouds under consideration, 240 synthetic stratocumulus clouds were generated. Each of these synthetic cloud collections was based on eight random number seeds and five sets of parameter values for each of six fractal parameters, as indicated in Table 2.

An outcome of comparing synthetic and real clouds was that errors did not change significantly with variations in the internal fractal parameters (that is, internal Hurst parameter, internal lacunarity, and internal lattice resolution).

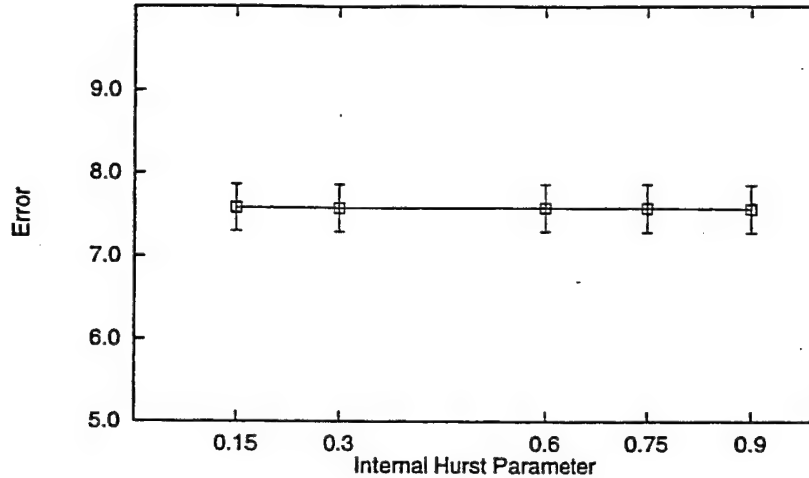[1]The L_2 norm of e_1, e_2, and e_3 is $\sqrt{e_1^2 + e_2^2 + e_3^2}$.

Figure 3: Error in synthetic clouds for several values of the internal Hurst parameter

Changes in horizontal parameters, on the other hand, did produce changes in errors that were significant relative to the standard deviations among the errors.

An example of the effect of changing an internal parameter is shown in Figure 3. This figure shows errors for several values of the internal Hurst parameter with error bars to indicate the standard deviations among the eight synthetic clouds generated by different random number seeds (for each value of internal Hurst parameter). The real-cloud collection against which the synthetic clouds were measured included all real cumulus images and used the corresponding metrics indicated in Table 1. As shown in Figure 3, the change in error with internal Hurst parameter is insignificant in consideration of the standard deviations.

Figure 4 shows the change in error with horizontal Hurst parameter. The three curves in the figure are associated with the real-cloud cumulus images due to the field experiment, the video images, and both image sources combined (which nearly coincides with the video image curve). There is a disparity in the magnitude of errors depending on the real-cloud collection used to establish the "correct" metric values. Note that the lower synthetic-cloud errors are associated with the larger collections of real clouds. This is because the greater variability in the larger real-cloud collections affected
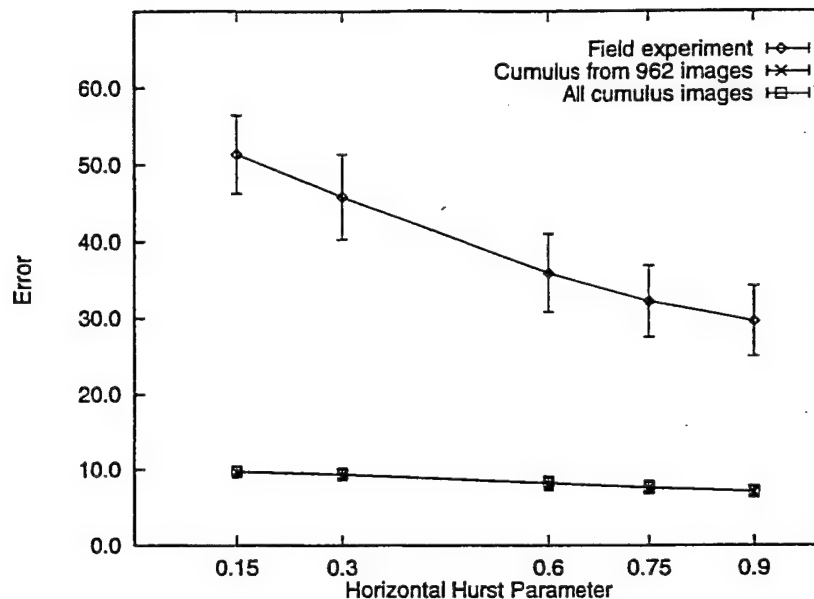
14

Figure 4: Error in synthetic clouds for several values of the horizontal Hurst parameter

the scaling of the metric values, in which a unit was defined by one standard deviation. For example, a greater variability in real clouds has a greater standard deviation resulting in a smaller scaling factor, equal to the inverse of the standard deviation. The outcome is smaller magnitude errors. Therefore, it is not appropriate to compare errors associated with different real-cloud collections for the purposes of studying sensitivity to fractal parameter values. What is important is the trend shown by each curve in consideration of the error bars.

The field experiment curve in Figure 4 indicates that the error can be reduced by increasing the horizontal Hurst parameter from its original value of 0.3. The other two curves from the figure are repeated in Figure 5 using an enlarged vertical scaling that shows the curves to have the same trend as the field experiment curve. The curves in Figures 4 and 5 show a $24 - 35\%$ reduction in error when the horizontal Hurst parameter is increased from 0.3 to 0.9.

Increasing the horizontal lattice resolution makes a negligible to small improvement in the error of the synthetic clouds. Figure 6 shows that er-
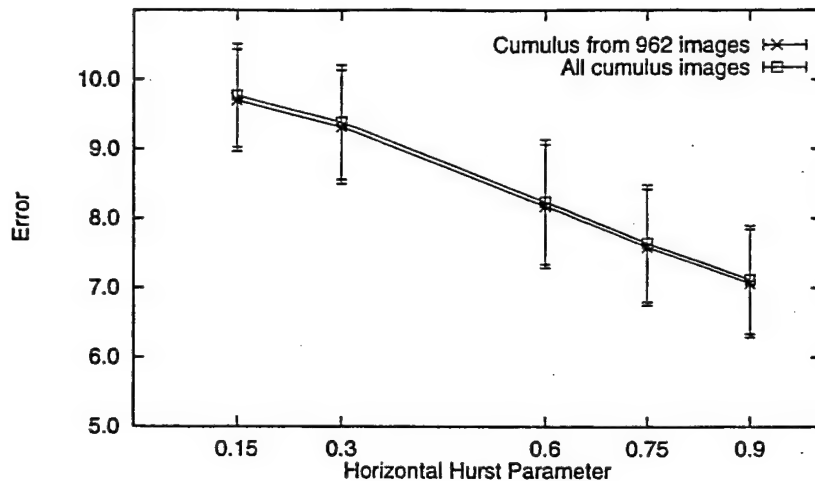
Figure 5: Error in synthetic clouds for several values of the horizontal Hurst parameter based on cumulus images from 962-image set and on all real cumulus images

ror decreases with increasing horizontal lattice resolution for the case where the field experiment data defines the correct cloud metrics. Note that the parameter values in the figure refer to the horizontal lattice resolution for the x direction, originally set at 6.0. Two of the curves from Figure 6 are shown on a different scale in Figure 7. These curves, which correspond to the larger real-cloud data sets, show a slight trend that is overshadowed by the error bars. Together the three real-cloud data sets weakly suggest that error reduction may be realized by increasing the horizontal lattice resolution from 6.0 to 9.0 (for the x direction, with the parameters for the other directions changed proportionally).

Figures 8 and 9 show that reducing the lacunarity from its original value of 3.0 lowers the error. Recall from Section 2.3.2 using $r = 1.0$ is not appropriate. The choice $r = 2.0$ lowers the error by $11 - 36$ % according the results represented in Figures 8 and 9.

In summary, when the fractal parameters are considered individually, the error is most sensitive to the horizontal Hurst parameter and the horizontal lacunarity. Specifically, the results given above suggest increasing the horizontal Hurst parameter and decreasing the horizontal lacunarity. It is interesting to note that both of these parameter changes are associated with
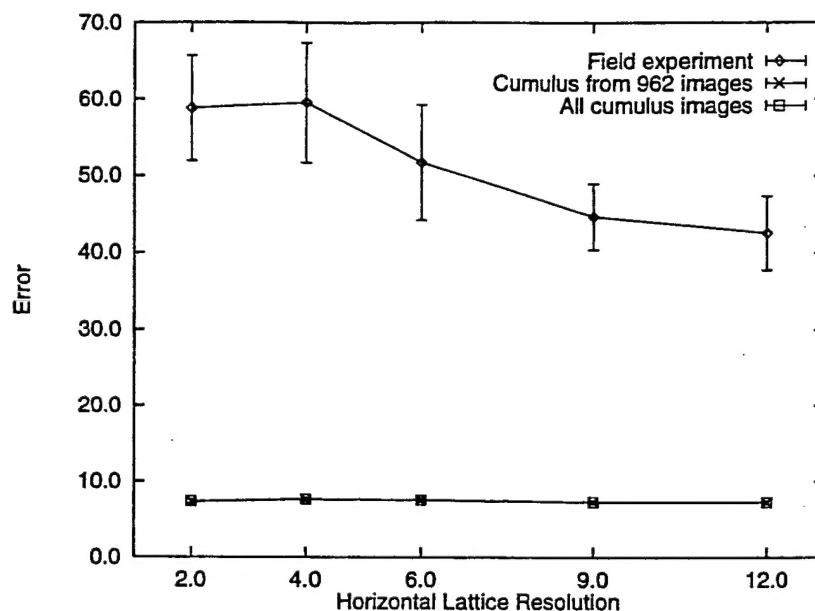
16

Figure 6: Error in synthetic clouds for several values of the horizontal lattice resolution
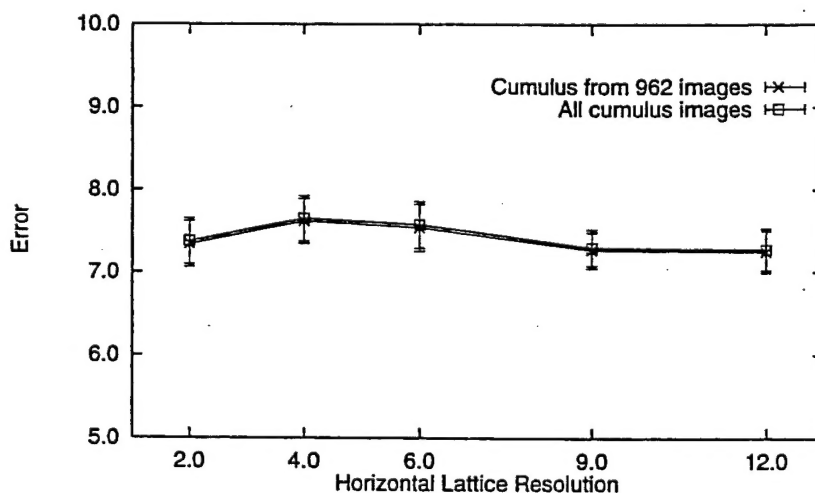

Figure 7: Error in synthetic clouds for several values of the horizontal lattice resolution based on cumulus images from 962-image set and on all real cumulus images
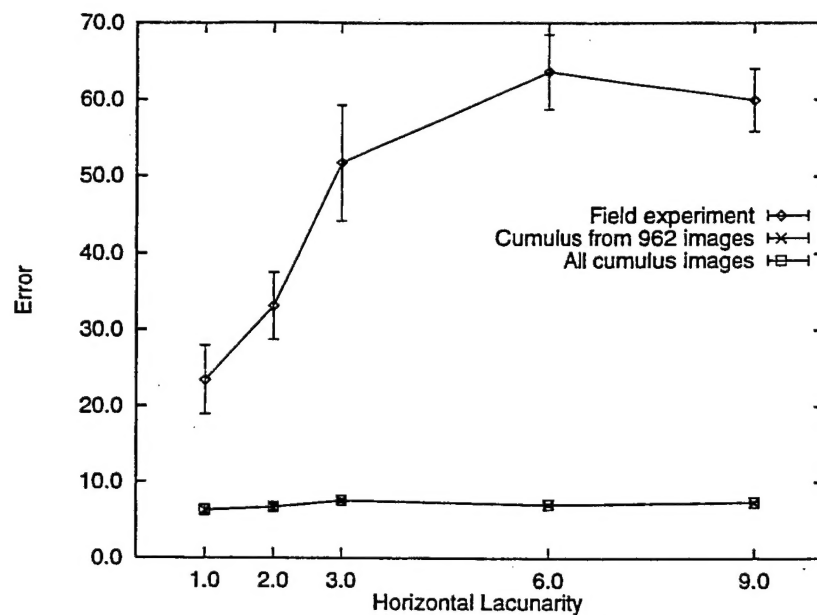
17

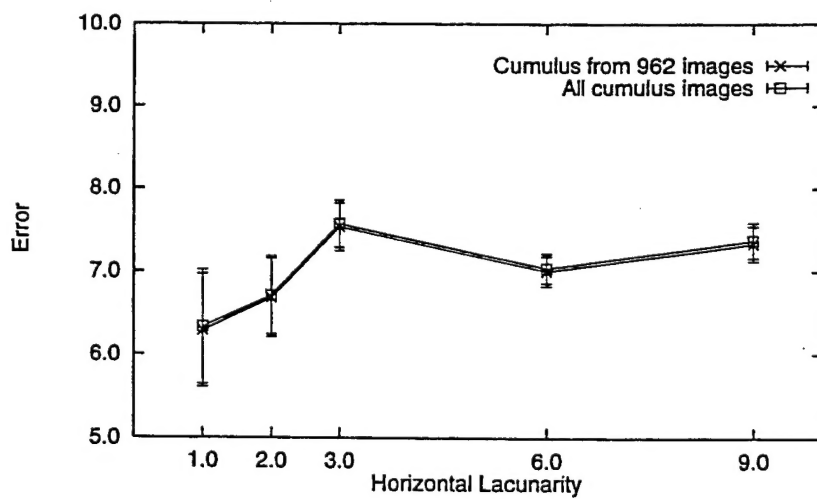Figure 8: Error in synthetic clouds for several values of the horizontal lacunarity

Figure 9: Error in synthetic clouds for several values of the horizontal lacunarity based on cumulus images from 962-image set and on all real cumulus images

18

a smoothing of small-scale features without a significant change to large-scale features. A third parameter change, an increase in the horizontal lattice resolution, is weakly suggested by this sensitivity study. Like the other parameter changes indicated by this study, increasing the horizontal lattice resolution would smooth the small-scale variations.

The three parameter changes indicated by this sensitvity study were made simultaneously. The result was that the error was reduced further than when the parameters were changed individually. When the horizontal Hurst parameter is set to 0.9, the horizontal lattice resolution is set to 12.0, and the horizontal lacunarity is set to 2.0, the error is $36-51\%$ lower than when the original parameter values are used. This suggests that improvements observed when one parameter is adjusted can be enhanced by adjusting other parameters simultaneously.

2.5   RESULTS AND CONCLUSIONS

The qualitative effects of adjusting CSSM parameters have been predicted. These predictions are in agreement with the images and the image-based observations in [3] made by TASC. Candidate parameters for adjustment were selected from a large number of parameters to limit the computation time required.

An error calculation method that uses any number of selected metrics and a collection of real-cloud imagery was devised to evaluate radiometric accuracy. The error obtained in this way is only meaningful when considered in terms of the real-cloud collection used to establish the error. In other words, it is a measure of relative error. Based on such errors, the sensitivities of the different parameters were assessed.

It was found that significant improvements in error could be achieved when the horizontal Hurst parameter was increased or the horizontal lacunarity was decreased. Negligible to small improvements could be obtained by increasing the horizontal lattice resolution. When all three adjustments were made simultaneously the error was reduced more than it was by any of the individual parameter adjustments.

All of the parameter adjustments indicated by the present study produce a smoothing of small-scale features without significantly changing large-scale features. This implies that the CSSM images are in better agreement with the real-cloud images when the high-frequency, or small-scale, features are reduced. This is a reflection of the inability of the real-cloud imagery to

BIBLIOGRAPHY

[1] Ayer, S. M., Gordon, S. C., Mozer, J. B., Seeley, G., and Triantafillou, S. A. (1999) *Radiometric Validation of the Cloud Scene Simulation Model*, to be published as AFRL Technical Report, Hanscom AFB, MA.

[2] Cianciolo, M. E., Raffensberger, M. E.., Schimdt, E. O, and Stearns, J. R. (1996) *Atmospheric Scene Simulation Modeling and Visualization*, PL-TR-96-2079, TASC, Reading, MA.   (AD # A312179)

[3] Cianciolo, M. E. and Rasmussen, R. G. (1992) *Cloud scene simulation modeling, the enchanced model*, PL-TR-92-2106, TASC, Reading, MA. (AD # A265958)

[4] Feddes, R. G. Complete this reference using Ref. 9 from TASC, 1996 report, if it is needed here (referenced in CSSM description).

[5] Saupe, D., Point evaluation of multi-variable random fractals, in *Visualisierung in Mathematik and Naturwissenschaft*, H. Jurgens and D. Saupe (eds.), Springer-Verlag, Heidelberg, 1989.

[6] Smalley, D. J. and Mozer, J. B. (1999) *Prioritized Performance Improvements of NPOESS Meteorological Sensors*, to be published as AFRL Technical Report, Hanscom AFB, MA.

[7] Turkington, R. B., Cianciolo, M. E., and Raffensberger, M. E. (1998) *Atmospheric scene simulation modeling and visualization*, TR-08607-1, TASC, Reading, MA.